J Biomol NMR (2011) 51:293–302
DOI 10.1007/s10858-011-9536-y

ARTICLE

Evaluation of the influence of intermolecular electron-nucleus couplings and intrinsic metal binding sites on the measurement of ^{15}N longitudinal paramagnetic relaxation enhancements in proteins by solid-state NMR

Philippe S. Nadaud · Ishita Sengupta · Jonathan J. Helmus · Christopher P. Jaroniec

Received: 20 June 2011 / Accepted: 25 July 2011 / Published online: 9 August 2011

Abstract Magic-angle spinning solid-state NMR measurements of ^{15}N longitudinal paramagnetic relaxation enhancements (PREs) in ^{13}C,^{15}N-labeled proteins modified with Cu^{2+}-chelating tags can yield multiple long-range electron-nucleus distance restraints up to ~20 Å (Nadaud et al. in J Am Chem Soc 131:8108–8120, 2009). Using the EDTA-Cu^{2+} K28C mutant of B1 immunoglobulin binding domain of protein G (GB1) as a model, we investigate the effects on such measurements of intermolecular electron-nucleus couplings and intrinsic metal binding sites, both of which may potentially complicate the interpretation of PRE data in terms of the intramolecular protein fold. To quantitatively assess the influence of intermolecular ^{15}N-Cu^{2+} interactions we have determined a nearly complete set of longitudinal ^{15}N PREs for a series of microcrystalline samples containing ~10, 15 and 25 mol percent of the ^{13}C,^{15}N-labeled EDTA-Cu^{2+}-tagged protein diluted in a matrix of diamagnetic natural abundance GB1. The residual intermolecular interactions were found to be minor on the whole and account for only a fraction of the relatively small but systematic deviations observed between the experimental ^{15}N PREs and corresponding values calculated using protein structural models for residues furthest removed from the EDTA-Cu^{2+} tag. This suggests that these deviations are also caused in part by other factors not related to the protein structure, such as the presence in the protein of intrinsic secondary sites capable of binding Cu^{2+} ions. To probe this issue we performed a Cu^{2+} titration study for K28C-EDTA GB1 monitored by 2D ^{15}N-^{1}H solution-state NMR, which revealed that while for Cu^{2+}:protein molar ratios of $\leq$ 1.0 Cu^{2+} binds primarily to the high-affinity EDTA tag, as anticipated, at even slightly super-stoichiometric ratios the Cu^{2+} ions can also associate with side-chains of aspartate and glutamate residues. This in turn is expected to lead to enhanced PREs for residues located in the vicinity of the secondary Cu^{2+} binding sites, and indeed many of these residues were ones found to display the elevated longitudinal ^{15}N PREs in the solid phase.

Keywords Solid-state NMR · Magic-angle spinning · Paramagnetic relaxation enhancement · Pseudocontact shift · Spin label · Metal ion · Protein structure

Introduction

Magic-angle spinning (MAS) solid-state NMR spectroscopy has recently surfaced as a valuable technique for investigating, at the atomic-level, the molecular structure and dynamics of non-crystalline biological macromolecules that are not readily amenable to such analysis by other approaches (McDermott 2009; Böckmann and Meier 2010; Renault et al. 2010; Tycko 2011). One of the main outstanding challenges for the structural analysis of biomolecules by solid-state NMR is the relative dearth of unambiguous long-range (≥6 Å) distance restraints that can be derived from measurements of dipolar couplings involving ^{1}H, ^{13}C, ^{15}N and other nuclei. This challenge can potentially be surmounted for paramagnetic metalloproteins and diamagnetic proteins intentionally modified at specific sites with covalently-linked paramagnetic tags (Bertini et al. 2008; Otting

P. S. Nadaud · I. Sengupta · J. J. Helmus · C. P. Jaroniec (✉)
Department of Chemistry, The Ohio State University, 100 West 18th Avenue, Columbus, OH 43210, USA
e-mail: jaroniec@chemistry.ohio-state.edu

2010) by performing measurements of nuclear paramagnetic relaxation enhancements (PREs) and/or pseudocontact shifts, which can be of significant magnitude even for nuclei located up to ~20–25 Å away from the paramagnetic center (Bertini et al. 2001).

While paramagnetic NMR methods have been extensively utilized for the detailed analysis of biomacromolecular structure, dynamics and interactions in solution (Kosen 1989; Bertini et al. 2001, 2008; Ubbink et al. 2002; Jahnke 2002; Clore and Iwahara 2009; Otting 2010) the great majority of the early NMR investigations of paramagnetic biological solids have involved small molecule metal coordination complexes (Chacko et al. 1983; Walter and Oldfield 1987; Nayeem and Yesinowski 1988; Brough et al. 1993; Liu et al. 1995; Ishii et al. 2003; Zhang et al. 2005) and selectively labeled proteins (Lee and Oldfield 1982; Liu et al. 1998; Spooner et al. 1999; Jovanovic and McDermott 2005). More recently, however, multidimensional MAS solid-state NMR techniques have been successfully extended to uniformly ^{13}C,^{15}N-labeled peptides and proteins containing paramagnetic centers (Pintacuda et al. 2007; Su et al. 2008; Laage et al. 2009b; Wickramasinghe et al. 2007, 2009; Linser et al. 2009; Balayssac et al. 2007, 2008; Bertini et al. 2010a, b; Nadaud et al. 2007, 2009, 2010) for a variety of applications including measurements of long-range structural restraints in the form of pseudocontact shifts (Balayssac et al. 2007, 2008; Bertini et al. 2010a, b) and PREs (Nadaud et al. 2007, 2009, 2010).

In our previous studies of paramagnetic analogs of the B1 immunoglobulin binding domain of protein G (GB1) modified at specific residues with covalently-bound EDTA-Cu^{2+} tags, we have demonstrated that quantitative measurements of site-resolved longitudinal ^{15}N PREs by MAS solid-state NMR methods can yield multiple ^{15}N-Cu^{2+} distance restraints up to ~ 20 Å (Nadaud et al. 2009, 2010). Accurate interpretation of such ^{15}N PRE measurements in terms of the intramolecular protein fold relies on the ability to effectively suppress the effects of intermolecular electron-nucleus couplings, which is typically achieved by diluting the ^{13}C,^{15}N-labeled paramagnetic protein in a matrix of its diamagnetic natural abundance counterpart (Balayssac et al. 2007, 2008; Nadaud et al. 2007, 2009). Here, we present a set of experiments aimed at the thorough evaluation of the influence of residual intermolecular ^{15}N-Cu^{2+} couplings on the analysis of longitudinal ^{15}N PRE data in proteins using the EDTA-Cu^{2+} K28C mutant of GB1 as a model system. In addition, we probe for the presence of intrinsic Cu^{2+} protein binding sites in K28C-EDTA GB1 by solution-state NMR spectroscopy, and consider the influence of such sites on the measurement and interpretation of PRE data in the solid phase.

Materials and methods

Protein sample preparation for solid-state NMR

Natural abundance GB1 and uniformly ^{13}C,^{15}N-labeled K28C mutant of GB1 were expressed according to previously published protocols (Nadaud et al. 2007, 2009, 2010) using *Escherichia coli* BL21(DE3) with Luria–Bertani and ^{13}C,^{15}N-enriched minimal medium, respectively, followed by gel filtration chromatography purification. The EDTA-Cu^{2+} side-chain was introduced into K28C-GB1 using thiol-disulfide chemistry, by reacting the protein with N-[S-(2-pyridylthio)cysteaminyl]EDTA (Ebright et al. 1992; Ermácora et al. 1992) (Toronto Research Chemicals) preloaded with 1.1 molar equivalents of Cu^{2+} (Nadaud et al. 2009). Diamagnetic control ^{13}C,^{15}N-labeled K28C-GB1 containing an EDTA-Zn^{2+} side-chain was prepared in analogous fashion.

Protein microcrystals for solid-state NMR analysis were prepared as described previously (Nadaud et al. 2009), by co-precipitating the ^{13}C,^{15}N-enriched EDTA-Cu^{2+} and EDTA-Zn^{2+} proteins with natural abundance GB1 using microdialysis at 4°C and a precipitant solution containing 2-methylpentane-2,4-diol, isopropanol, and deionized water in a 2:1:1 (v/v) ratio. For both EDTA-Cu^{2+} and EDTA-Zn^{2+} proteins a series of samples were prepared with EDTA-Cu^{2+}/Zn^{2+}:GB1 molar ratios of ca. 1:3, 1:6 and 1:9, corresponding to ca. 25, 15 and 10 mol percent of the ^{13}C,^{15}N-EDTA-Cu^{2+}/Zn^{2+} protein, respectively. In the following, the K28C-GB1 EDTA-Cu^{2+}/Zn^{2+} protein samples described above will be referred to as 28EDTA-Cu^{2+}/Zn^{2+}-25, 28EDTA-Cu^{2+}/Zn^{2+}-15 and 28EDTA-Cu^{2+}/Zn^{2+}-10. For each sample a total of ~ 5 mg of protein microcrystals were packed into a 1.6 mm zirconia rotor (Agilent Technologies), corresponding to ~1.2, 0.7 and 0.5 mg of ^{13}C,^{15}N-labeled protein for the 28EDTA-Cu^{2+}/Zn^{2+}-25, 28EDTA-Cu^{2+}/Zn^{2+}-15 and 28EDTA-Cu^{2+}/Zn^{2+}-10 samples, respectively. The amounts of ^{13}C,^{15}N-labeled proteins were confirmed by a quantitative comparison of the spectral intensities with a control sample containing a known amount of ^{13}C,^{15}N-28EDTA-Cu^{2+}.

Solid-state NMR spectroscopy

Experiments were performed on a three-channel 11.7 T Varian spectrometer operating at frequencies of 499.8 MHz for ^{1}H, 125.7 MHz for ^{13}C and 50.6 MHz for ^{15}N, equipped with a 1.6 mm FastMAS™ probe. The MAS rate was set to 40 kHz, regulated to ca. ± 20 Hz using a MAS control unit, and the effective sample temperature was maintained at ~5°C using a variable temperature stack and control unit. Spectra were processed with NMRPipe (Delaglio et al. 1995) and analyzed using home-built software.

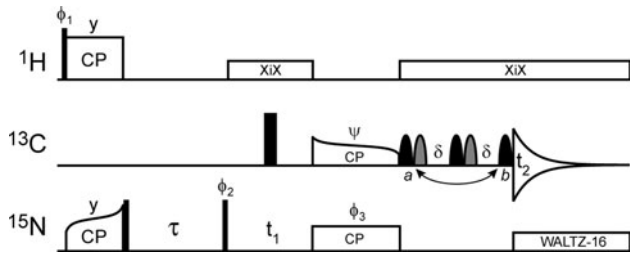

Fig. 1 2D NCO-S^3E based pulse scheme used to determine the residue-specific longitudinal ^{15}N relaxation rate constants. Narrow and wide black rectangles correspond to 90° and 180° pulses, respectively, and all pulses have phase *x* unless indicated otherwise. The ^{1}H, ^{13}C and ^{15}N carriers were placed at 4.7, 175, and 120 ppm, respectively (additional experimental parameters are given in the "Materials and methods" section). The S^3E ^{13}CO-$^{13}C\alpha$ J-decoupling scheme, with the delay $\delta = 2.25$ ms, consisted of two separate spectra recorded with selective rSNOB 180° pulses (Kupce et al. 1995) of 250 μs duration applied to the ^{13}CO spins at the frequency of 175 ppm (*filled black shapes*) and $^{13}C\alpha$ spins at the frequency of 55 ppm (*filled gray shapes*) in either position *a* or *b*. The spectra were processed as described by Laage et al. (2009a). The following phase cycles were employed to record spectra *a* and *b*. Spectrum *a*: $\varphi_1 = 2(x), 2(-x)$; $\varphi_2 = x, -x$; $\varphi_3 = y$; $\psi = x$; receiver $= x, -x, -x, x$. Spectrum *b*: $\varphi_1 = 2(x), 2(-x)$; $\varphi_2 = x, -x$; $\varphi_3 = y$; $\psi = -y$; receiver $= x, -x, -x, x$. Quadrature in the ^{15}N dimension was achieved by alternating phase φ_2 according to the States method (States et al. 1982)

Residue-specific amide ^{15}N longitudinal relaxation rate constants, R_1, were determined for the 28EDTA-Cu^{2+}/Zn^{2+} samples using the 2D NCO-S^3E based pulse scheme shown in Fig. 1 and described in detail previously (Nadaud et al. 2010), with ten values of the relaxation delay, τ, ranging from ~0 to 4 s. Briefly, ^{1}H-^{15}N cross-polarization (Pines et al. 1973) was achieved by using ~60 kHz ^{15}N field applied with a tangential ramp (Hediger et al. 1995), ~100 kHz ^{1}H field, and contact time of 0.9 ms. The SPECIFIC CP scheme (Baldus et al. 1998), employing ~15 kHz ^{15}N field, ~25 kHz ^{13}C field with a tangential ramp, and 7 ms contact time, was used to transfer magnetization from ^{15}N to ^{13}CO spins. ^{13}CO-$^{13}C\alpha$ J-decoupling during ^{13}CO detection was accomplished using the S^3E element (Laage et al. 2009a), and XiX (Detken et al. 2002) and WALTZ-16 (Shaka et al. 1983) decoupling schemes were applied at field strengths of ~12 kHz and ~3.3 kHz, respectively, on the ^{1}H and ^{15}N channels as shown in Fig. 1 (see the figure caption for additional pulse scheme details). The recycle delays employed were set to three times ^{1}H T_1, i.e., ~0.4 s and ~1.3 s for the 28EDTA-Cu^{2+} and 28EDTA-Zn^{2+} samples, respectively, and the total experiment times used to record the residue-specific ^{15}N R_1 trajectories ranged from ~60 h to ~240 h for the 28EDTA-Zn^{2+}-25 and 28EDTA-Cu^{2+}-10 samples, respectively. For each residue in K28C-GB1 the longitudinal ^{15}N PRE (also denoted in the following as Γ_1^N) was obtained by calculating the difference between the ^{15}N R_1 values for the 28EDTA-Cu^{2+}-25/15/10 samples and 28EDTA-Zn^{2+}-25, found by modeling the individual relaxation trajectories as single exponential decays. Note that, as expected, for the diamagnetic 28EDTA-Zn^{2+}-25/15/10 samples the ^{15}N R_1 rates were found to be independent within experimental error of the dilution ratio for the ^{13}C,^{15}N-labeled EDTA-Zn^{2+} tagged protein (data not shown). Thus, the ^{15}N PRE calculations used the 28EDTA-Zn^{2+}-25 data having the highest signal-to-noise ratio.

Cu^{2+} titration of K28C-EDTA GB1 monitored by solution-state NMR spectroscopy

The binding of Cu^{2+} to K28C-EDTA GB1 was probed by using a series of samples each consisting of an aqueous solution of 0.40 mM ^{15}N-K28C-EDTA GB1 and 7% D_2O at pH 7.0, containing increasing amounts of $CuCl_2$. The $CuCl_2$ concentrations used were 0, 0.08, 0.16, 0.24, 0.32, 0.40, 0.48, 0.56, 0.64, 0.72 mM corresponding to Cu^{2+}:protein molar ratios of 0, 0.2, 0.4, 0.6, 0.8, 1.0, 1.2, 1.4, 1.6, 1.8, respectively. For each sample in the series, a gradient and sensitivity enhanced two dimensional ^{15}N-^{1}H heteronuclear single quantum coherence (HSQC) NMR spectrum (Kay et al. 1992) was recorded at 25°C on a 600 MHz Bruker DMX spectrometer, equipped with a room temperature probe with triple-axis gradients. Data were processed with NMRPipe (Delaglio et al. 1995) and analyzed using Sparky version 3.113 (Goddard and Kneller 2006).

Results and discussion

Evaluation of the influence of intermolecular electron-nucleus couplings on the measurement of longitudinal ^{15}N PREs in proteins

The interpretation of longitudinal ^{15}N PRE measurements in the solid phase in terms of the intramolecular protein fold relies on the ability to account for or effectively suppress the effects of intermolecular electron-nucleus couplings. In our previous experiments on paramagnetic EDTA-Cu^{2+} GB1 analogs (Nadaud et al. 2009, 2010) this was achieved by preparing microcrystalline samples consisting of ~25–30 mol percent of the ^{13}C,^{15}N-labeled EDTA-Cu^{2+}-tagged protein diluted in a matrix of its natural abundance diamagnetic counterpart—a compromise between the dilution factor and reasonably high spectral signal-to-noise ratio. While this approach was generally successful in attenuating the intermolecular PRE effects it also became apparent that for a subset of residues for which the available protein structural models suggested the presence of very small longitudinal ^{15}N PREs

($\Gamma_1^N \leq 0.05\ s^{-1}$), the experimentally determined PRE values systematically exceeded the corresponding predicted ones, by as much as $\sim$0.2–0.3 s^{-1} in several cases.

To assess the degree to which residual intermolecular ^{15}N-Cu^{2+} interactions can be expected to be responsible for such discrepancies we have performed systematic measurements of longitudinal ^{15}N PREs for a series of samples of a model protein, ^{13}C,^{15}N-labeled EDTA-Cu^{2+} K28C mutant of GB1, diluted in a matrix of natural abundance GB1 at ratios of $\sim$10, 15 and 25 mol percent. In Fig. 2 we show representative 2D ^{15}N-^{13}CO correlation spectra recorded for the 28EDTA-Cu^{2+}-25 and 28EDTA-Cu^{2+}-10 samples, where the resonance assignments have been established previously (Nadaud et al. 2010) and verified here using 2D and 3D solid-state NMR chemical shift correlation experiments. From these data it is evident that the combination of high MAS rate, optimized low power pulse scheme and short recycle delays yields high resolution and sensitivity spectra within several hours for samples containing as little as $\sim$75 nmol ($\sim$0.5 mg) of ^{13}C,^{15}N-labeled protein. In order to determine the residue-specific longitudinal ^{15}N relaxation rates for the 28EDTA-Cu^{2+}-25/15/10 samples, a series of 2D ^{15}N-^{13}CO correlation spectra analogous to those shown in Fig. 2 were recorded for each sample as a function of the relaxation delay, τ (see Fig. 1). Representative relaxation trajectories for residues L7, A24, G41 and E42 in 28EDTA-Cu^{2+}-25/15/10, located in different regions of the protein, are shown in Fig. 3 along with the corresponding trajectories for the diamagnetic 28EDTA-Zn^{2+}-25 control sample. A qualitative inspection of these data reveals that while for certain residues (L7 and A24) the intermolecular PRE contributions appear to be negligible as evidenced by the nearly identical relaxation trajectories, for others (G41 and E42) the relaxation trajectories for the least dilute EDTA-Cu^{2+} sample (28EDTA-Cu^{2+}-25) differ noticeably from those obtained for samples containing 10 and 15% of the ^{13}C,^{15}N-EDTA-Cu^{2+} protein due to the attenuation of residual intermolecular ^{15}N-Cu^{2+} interactions.

The residue-specific ^{15}N PREs were calculated according to $\Gamma_1^N = R_1(Cu^{2+}) - R_1(Zn^{2+})$, where the R_1 values for the EDTA-Cu^{2+} and Zn^{2+} tagged proteins were obtained by fitting the relaxation trajectories to single exponential decays. The results are listed in Table 1 and summarized in Fig. 4, where the PREs determined for the 28EDTA-Cu^{2+}-25/15/10 samples are plotted as a function of residue number and mapped onto the tertiary structure of GB1. These data show that: (1) as expected, the largest PREs (colored in red in the plots and structures) are associated with α-helical amino acid residues $\sim$24–32 closest to the EDTA-Cu^{2+} tag, and (2) several residues distant from the paramagnetic tag, most prominently D40-W43, display anomalously elevated PRE values for the 28EDTA-Cu^{2+}-25 sample. While the dilution of the ^{13}C,^{15}N-EDTA-Cu^{2+} protein in the diamagnetic matrix to $\sim$10–15 mol percent has no significant effect on the largest PREs for the α-helix residues, it is evident that it leads to some attenuation of the PREs for amino acids in strands β1–β4 and intervening loops, located further away from the paramagnetic Cu^{2+} center. In order to rapidly visualize the effectiveness of the dilution procedure in suppressing the residual intermolecular ^{15}N-Cu^{2+} couplings, in Fig. 5 we show correlation plots which compare the ^{15}N PRE data recorded for 28EDTA-Cu^{2+}-25 and 28EDTA-Cu^{2+}-15 with those for the most dilute 28EDTA-Cu^{2+}-10 sample. From this comparison it is clear that the smallest PREs

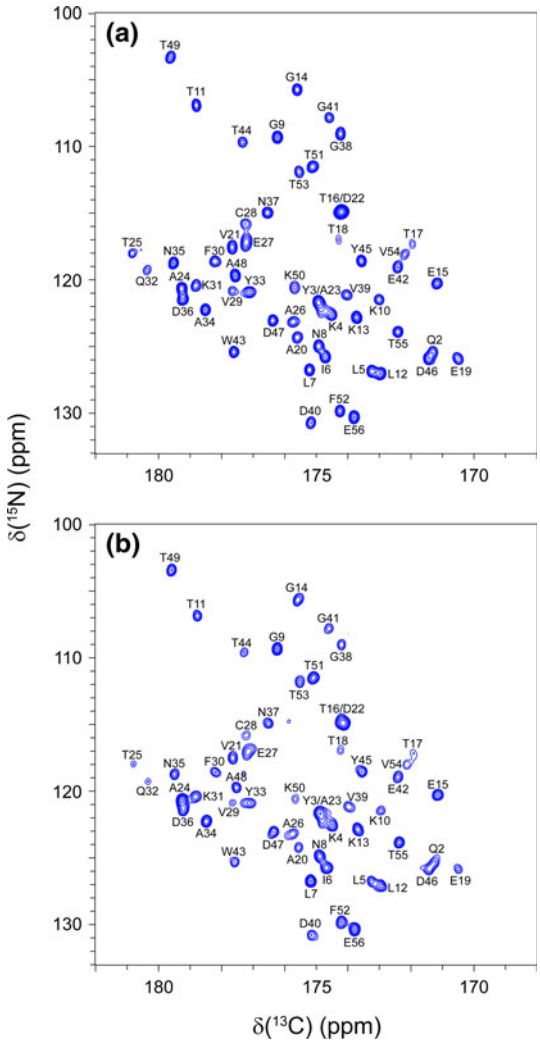

Fig. 2 ^{15}N-^{13}CO solid-state NMR chemical shift correlation spectra of **a** 28EDTA-Cu^{2+}-25 and **b** 28EDTA-Cu^{2+}-10 samples recorded at 11.7 T and 40 kHz MAS frequency using the 2D NCO-S^{3}E pulse scheme (Laage et al. 2009a). The spectra in panels **a** and **b** were recorded in $\sim$2 and $\sim$6 h, respectively, with $t_{1,max}(^{15}N) = 25.6$ ms and $t_{2,max}(^{13}C) = 30$ ms, and processed with 81°-shifted sine-bell window functions in F_1 and F_2. The resonance assignments have been established previously (Nadaud et al. 2010)

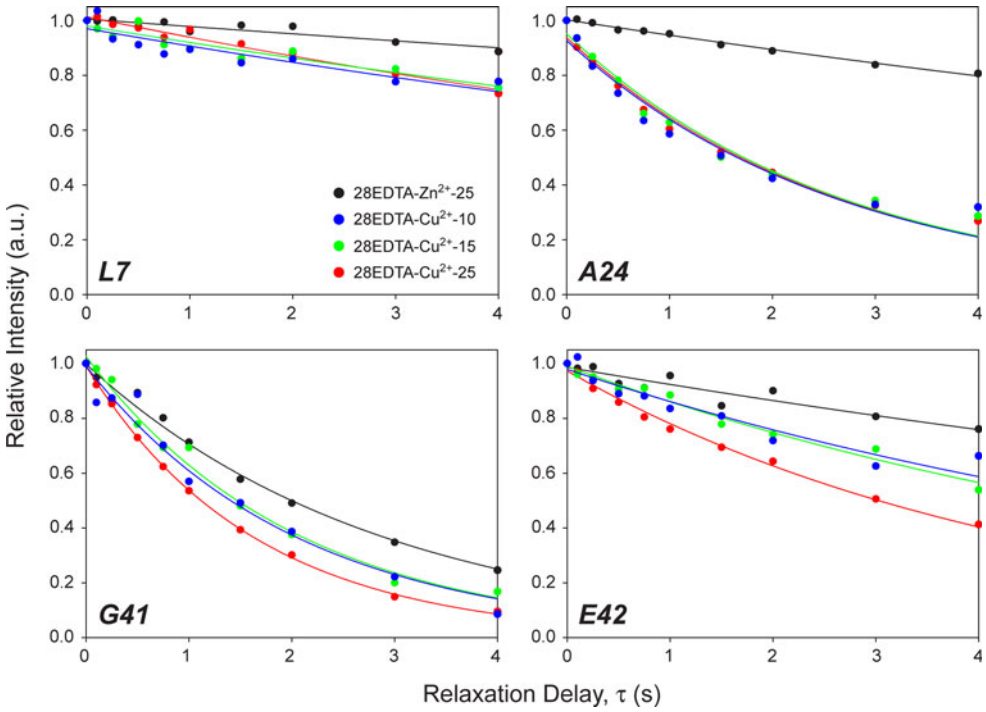

Fig. 3 Representative solid-state NMR measurements of backbone amide ^{15}N longitudinal relaxation rates, R_1, for 28EDTA-Zn^{2+}-25 (*black*), 28EDTA-Cu^{2+}-10 (*blue*), 28EDTA-Cu^{2+}-15 (*green*) and 28EDTA-Cu^{2+}-25 (*red*). The relaxation trajectories were recorded using the pulse scheme shown in Fig. 1 by varying the relaxation delay, τ. Best-fits to decaying single exponentials are shown as *solid lines*

($\Gamma_1^N < 0.1\ s^{-1}$)—which are expected to be subject to the most significant contamination by intermolecular effects—determined for the 28EDTA-Cu^{2+}-10 sample are quite similar to the corresponding values for 28EDTA-Cu^{2+}-15 and systematically smaller than those for 28EDTA-Cu^{2+}-25. For the subset of PRE values corresponding to $\Gamma_1^N < 0.1\ s^{-1}$ in 28EDTA-Cu^{2+}-10 a quantitative comparison yields average PRE deviations, $\Delta\Gamma_1^N$, between the 28EDTA-Cu^{2+}-25/15 and 28EDTA-Cu^{2+}-10 samples of $0.030 \pm 0.023\ s^{-1}$ and $0.011 \pm 0.016\ s^{-1}$ for 28EDTA-Cu^{2+}-25 and 28EDTA-Cu^{2+}-15, respectively, where for each residue the PRE differences were calculated as $\Delta\Gamma_1^N = \Gamma_1^N$(28EDTA-$Cu^{2+}$-25/15) – Γ_1^N(28EDTA-Cu^{2+}-10). Altogether, the data in Figs. 4 and 5 indicate that: (1) residual intermolecular ^{15}N-Cu^{2+} couplings do contribute to a small degree to elevated ^{15}N PRE values observed for a subset of residues distant from the paramagnetic tag for the least dilute 28EDTA-Cu^{2+}-25 sample, and (2) these residual intermolecular couplings are effectively quenched by diluting the ^{13}C,^{15}N-EDTA-Cu^{2+} protein in the diamagnetic matrix to ~10–15 mol percent.

Characterization of intrinsic protein metal binding sites and their potential impact on ^{15}N PRE measurements

A closer inspection of the data in Fig. 4 suggests that residual intermolecular ^{15}N-Cu^{2+} interactions are not the sole factor responsible for the anomalous systematic increase in the measured ^{15}N PREs for certain residues in 28EDTA-Cu^{2+}. For instance, while the most dilute 28EDTA-Cu^{2+}-10 sample clearly displays attenuated PRE values for residues D40-W43 relative to 28EDTA-Cu^{2+}-25 these residues continue to display considerable ^{15}N PREs, in the ~0.05–0.15 s^{-1} range [corresponding to ^{15}N-Cu^{2+} distances of ~14–17 Å according to calculations using the Solomon-Bloembergen equation (Solomon 1955; Bloembergen and Morgan 1961)], which are highly unlikely to report on their proximity to the EDTA-Cu^{2+} tag and hence the protein structure. To gain further insight into this issue, in Fig. 6 we compare the experimentally observed ^{15}N PREs for 28EDTA-Cu^{2+}-25/15/10 with the corresponding values calculated from structural models of 28EDTA-Cu^{2+} constructed based on the atomic coordinates of GB1 using Xplor-NIH (Schwieters et al. 2003). On the whole, reasonable agreement is obtained between the experimental PREs and those predicted by the protein structural models—note that the seemingly significant deviations seen for a few Γ_1^N values $\geq 0.2\ s^{-1}$ are in fact largely inconsequential for applications to protein structural studies due to the very strong dependence of the PRE value on the ^{15}N-Cu^{2+} distance in this regime (e.g., the difference in ^{15}N-Cu^{2+} distances corresponding to PRE values of 0.2 and 0.6 s^{-1} is only ~2 Å). On the other hand, notable systematic deviations between the observed and calculated Γ_1^N values are seen for a cluster of measurements corresponding to calculated $\Gamma_1^N \leq 0.05\ s^{-1}$, as already observed in the context of our previous studies (Nadaud et al. 2009, 2010). Most significant, however, is the finding that although somewhat reduced for the 28EDTA-Cu^{2+}-15 and 28EDTA-Cu^{2+}-10 samples in comparison with

Table 1 Backbone amide ^{15}N longitudinal PREs, Γ_1^N, determined for the 28EDTA-Cu^{2+}-25, 28EDTA-Cu^{2+}-15, and 28EDTA-Cu^{2+}-10 samples

Residue	Γ_1^N (s^{-1})		
	28EDTA-Cu^{2+}-25	28EDTA-Cu^{2+}-15	28EDTA-Cu^{2+}-10
Q2	0.062 ± 0.006	0.043 ± 0.013	0.020 ± 0.007
Y3	–[a]	–	–
K4	0.079 ± 0.010	0.051 ± 0.008	0.024 ± 0.010
L5	0.038 ± 0.007	0.013 ± 0.010	0.026 ± 0.015
I6	0.041 ± 0.006	0.041 ± 0.006	0.014 ± 0.005
L7	0.048 ± 0.006	0.036 ± 0.009	0.040 ± 0.013
N8	0.037 ± 0.006	0.033 ± 0.007	0.023 ± 0.012
G9	0.052 ± 0.008	0.018 ± 0.009	0.015 ± 0.008
K10	0.090 ± 0.012	0.047 ± 0.014	0.035 ± 0.014
T11	0.063 ± 0.009	0.030 ± 0.013	0.038 ± 0.014
L12	0.065 ± 0.007	0.033 ± 0.013	0.018 ± 0.013
K13	0.034 ± 0.007	0.028 ± 0.013	0.009 ± 0.011
G14	0.041 ± 0.008	0.024 ± 0.010	0.015 ± 0.012
E15	0.055 ± 0.009	0.036 ± 0.013	0.011 ± 0.015
T16	–	–	–
T17	0.063 ± 0.019	0.008 ± 0.018	0.019 ± 0.023
T18	0.027 ± 0.020	0.040 ± 0.021	0.019 ± 0.016
E19	0.063 ± 0.013	0.080 ± 0.013	0.047 ± 0.024
A20	0.080 ± 0.011	0.080 ± 0.016	0.070 ± 0.017
V21	0.130 ± 0.013	0.117 ± 0.020	0.127 ± 0.021
D22	–	–	–
A23	–	–	–
A24	0.315 ± 0.024	0.32 ± 0.03	0.32 ± 0.04
T25	0.85 ± 0.06	0.97 ± 0.08	0.73 ± 0.07
A26	0.243 ± 0.015	0.227 ± 0.013	0.187 ± 0.015
E27	0.211 ± 0.014	0.213 ± 0.016	0.18 ± 0.03
C28	0.45 ± 0.06	0.42 ± 0.05	0.36 ± 0.07
V29	0.50 ± 0.03	0.44 ± 0.05	0.43 ± 0.06
F30	0.242 ± 0.011	0.271 ± 0.020	0.22 ± 0.03
K31	0.43 ± 0.03	0.36 ± 0.03	0.34 ± 0.03
Q32	0.56 ± 0.04	0.66 ± 0.08	0.58 ± 0.09
Y33	0.196 ± 0.011	0.205 ± 0.021	0.173 ± 0.012
A34	0.126 ± 0.010	0.133 ± 0.013	0.148 ± 0.014
N35	0.187 ± 0.012	0.170 ± 0.012	0.166 ± 0.021
D36	0.133 ± 0.008	0.151 ± 0.021	0.140 ± 0.019
N37	0.069 ± 0.009	0.077 ± 0.014	0.051 ± 0.018
G38	0.059 ± 0.009	0.043 ± 0.012	0.014 ± 0.017
V39	0.076 ± 0.009	0.035 ± 0.015	0.052 ± 0.019
D40	0.182 ± 0.015	0.134 ± 0.017	0.12 ± 0.03
G41	0.266 ± 0.019	0.14 ± 0.03	0.14 ± 0.05
E42	0.155 ± 0.012	0.074 ± 0.012	0.062 ± 0.017
W43	0.187 ± 0.012	0.144 ± 0.024	0.120 ± 0.024
T44	0.095 ± 0.014	0.077 ± 0.016	0.056 ± 0.025
Y45	0.075 ± 0.009	0.062 ± 0.013	0.063 ± 0.016
D46	0.067 ± 0.006	0.050 ± 0.008	0.030 ± 0.013
D47	0.042 ± 0.011	0.051 ± 0.011	0.059 ± 0.014
A48	0.057 ± 0.008	0.051 ± 0.010	0.052 ± 0.016
T49	0.036 ± 0.011	0.011 ± 0.013	−0.030 ± 0.017
K50	0.062 ± 0.015	0.039 ± 0.016	0.044 ± 0.024
T51	0.055 ± 0.008	0.043 ± 0.008	0.000 ± 0.011
F52	0.037 ± 0.007	0.028 ± 0.019	0.025 ± 0.015
T53	0.056 ± 0.012	0.042 ± 0.013	0.033 ± 0.020
V54	0.034 ± 0.013	0.008 ± 0.015	0.027 ± 0.014
T55	0.050 ± 0.007	0.031 ± 0.006	0.037 ± 0.017
E56	0.109 ± 0.010	0.055 ± 0.009	0.035 ± 0.011

[a] PRE value could not be determined due to spectral overlap

28EDTA-Cu^{2+}-25—the average differences between observed and calculated PREs for a subset of residues with calculated $\Gamma_1^N < 0.05\ s^{-1}$ were found to be 0.07 ± 0.05 s^{-1}, 0.05 ± 0.04 s^{-1}, and 0.04 ± 0.04 s^{-1} for 28EDTA-Cu^{2+}-25, 28EDTA-Cu^{2+}-15, and 28EDTA-Cu^{2+}-10, respectively—the systematic deviations between the observed and calculated PREs persist for all the protein samples regardless of the dilution ratio.

Considering the fact that the microcrystalline protein samples in this and our previous studies were prepared using a small, 1.1 molar equivalent, excess of Cu^{2+} ions to ensure complete occupation of the EDTA binding sites, one potential source of the above noted discrepancies between the measured and predicted PRE values could be the existence of secondary, weaker-affinity Cu^{2+} protein binding sites often associated with aspartate, glutamate and histidine residues (there are a total of 10 such residues in GB1 corresponding to positions E15, E19, D22, E27, D36, D40, E42, D46, D47 and E56). To directly probe for the presence of such binding sites in K28C-EDTA GB1 we performed a Cu^{2+} titration study monitored by 2D ^{15}N-^{1}H solution-state NMR as described in the "Materials and methods" section. In Fig. 7 we show small representative regions of ^{15}N-^{1}H HSQC spectra for K28C-EDTA GB1 recorded in the absence of Cu^{2+}, as well as in the presence of 1.0 and 1.2 molar equivalents of Cu^{2+}. We find that for the Cu^{2+}:protein molar ratio of 1.0 the resonance intensities for α-helix residues (e.g., V29 and Q32 in the spectra in Fig. 7) most proximal to the EDTA side-chain, i.e., the primary high-affinity Cu^{2+} binding site, are severely attenuated due to large transverse PREs while signals for the remaining residues are largely unaffected. On the other hand, for super-stoichiometric amounts of Cu^{2+} ([Cu^{2+}]:[protein] ≥ 1.2) additional residues far removed from the EDTA side-chain begin to experience

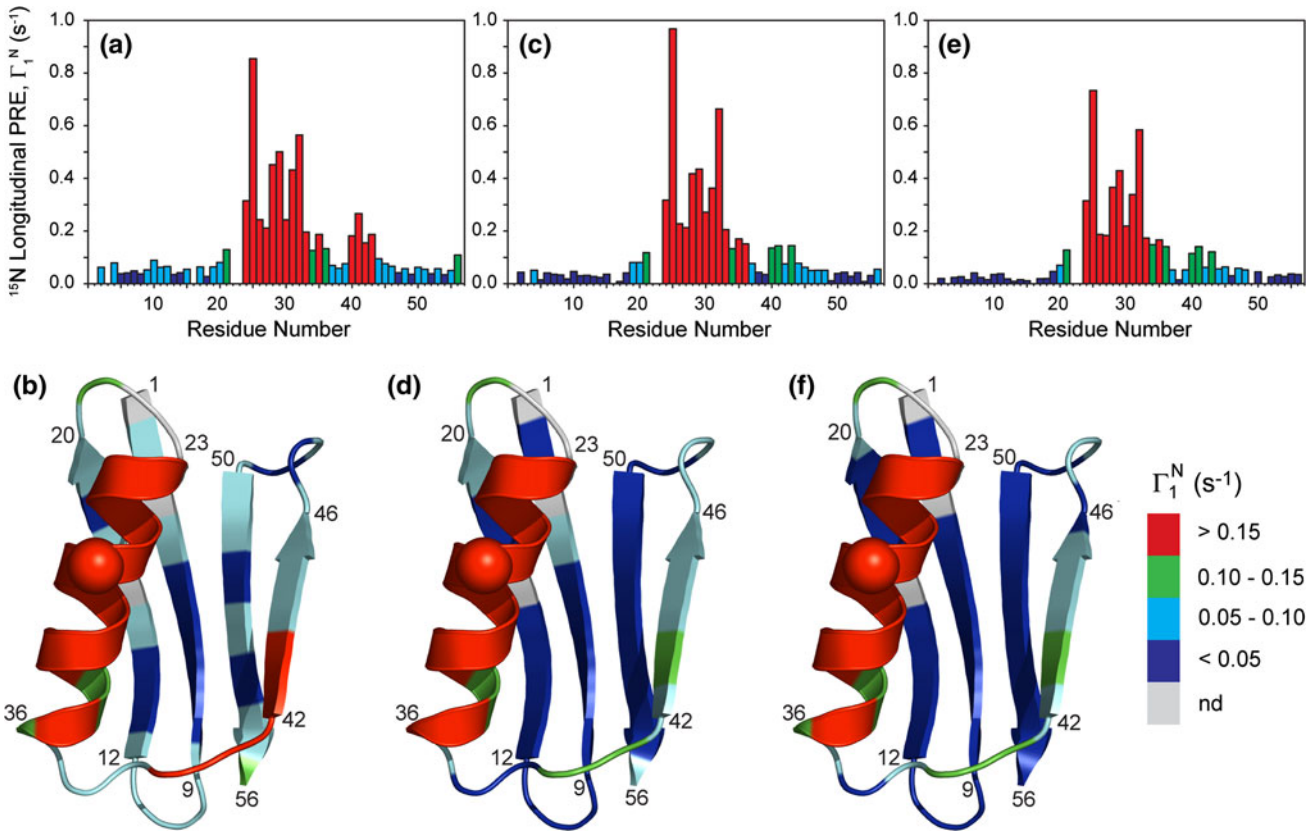

Fig. 4 Backbone amide ^{15}N longitudinal paramagnetic relaxation enhancements, $\Gamma_1^N = R_1(Cu^{2+}) - R_1(Zn^{2+})$, plotted as a function of residue number and mapped onto the tertiary structure of GB1 (PDB entry 1pga) for **a**, **b** 28EDTA-Cu^{2+}-25, **c**, **d** 28EDTA-Cu^{2+}-15 and **e**, **f** 28EDTA-Cu^{2+}-10. The location of the EDTA-Cu^{2+} tag at residue 28 is indicated by a *sphere*. The magnitudes of the measured residue-specific Γ_1^N values are color-coded in the plots and structures as indicated by the *color bar* on the right, according to the following scheme: $\Gamma_1^N > 0.15$ s^{-1} (*red*), $\Gamma_1^N = 0.10$–0.15 s^{-1} (*green*), $\Gamma_1^N = 0.05$–0.10 s^{-1} (*cyan*), and $\Gamma_1^N < 0.05$ s^{-1} (*blue*). Residues for which a Γ_1^N value could not be determined due to spectral overlap (Y3, T16, D22 and A23) are colored in *gray* in the structures, and the corresponding Γ_1^N values are set to zero in the plots

progressively increasing PRE effects due to the presence of Cu^{2+} ions, which is indicative of the existence of secondary Cu^{2+} binding sites in the protein. Analysis of the HSQC spectra reveals that residues most strongly affected at the higher Cu^{2+} concentrations indeed correspond to Asp and Glu as well as others located in their immediate spatial vicinity (e.g., Y3, E19, A20 and D40 in Fig. 7). This finding is consistent with the previously discussed solid-state NMR results, where many of the same residues were found to display the anomalously elevated longitudinal ^{15}N PREs. It is important to note here that only a minute fraction of the available secondary Cu^{2+} binding sites is likely to be occupied at any given time in the microcrystalline protein samples employed in the current study, with the Cu^{2+} ions in fast-exchange equilibrium with these binding sites and able to freely diffuse through the hydrated crystal framework. Nevertheless, the availability of such sites combined with the slight excess of Cu^{2+} used during sample preparation can locate paramagnetic Cu^{2+} ions within a few Å of the protein backbone for a small fraction of protein molecules. This in turn would generate extremely large PRE effects for the residues involved, with the overall result being the systematic elevation of the experimentally determined longitudinal ^{15}N PRE values for those sites.

Concluding remarks

Magic-angle spinning solid-state NMR measurements of nuclear paramagnetic relaxation enhancements and pseudocontact shifts in paramagnetic proteins can yield a multitude of restraints that are suitable for applications to protein structure determination (Balayssac et al. 2007, 2008; Bertini et al. 2010a, b; Nadaud et al. 2007, 2009, 2010). Given the long range nature of these restraints, their quantitative interpretation in terms of the intramolecular protein fold relies on the ability to properly account for or effectively suppress the effects of intermolecular electron-nucleus couplings. Here we have performed a systematic

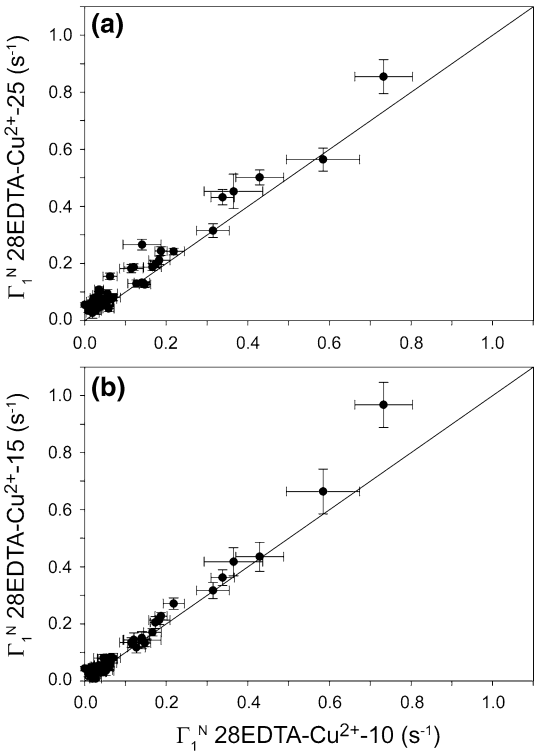

Fig. 5 Comparison of the residue-specific ^{15}N longitudinal PREs determined for 28EDTA-Cu^{2+}-10 with those for **a** 28EDTA-Cu^{2+}-25 and **b** 28EDTA-Cu^{2+}-15

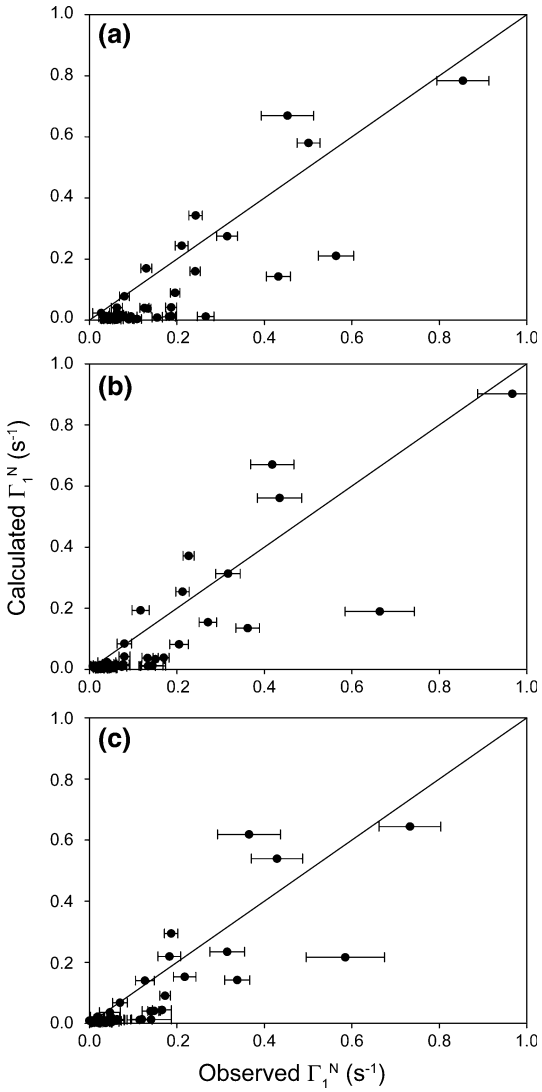

Fig. 6 Comparison between the experimentally determined ^{15}N longitudinal PREs and corresponding values calculated from protein structural models for **a** 28EDTA-Cu^{2+}-25, **b** 28EDTA-Cu^{2+}-15, and **c** 28EDTA-Cu^{2+}-10

evaluation of the influence of such intermolecular couplings on the measurements of longitudinal ^{15}N PREs in protein molecules intentionally modified with paramagnetic Cu^{2+}-chelating tags, using as a model system the EDTA-Cu^{2+} K28C mutant of B1 immunoglobulin binding domain of protein G in the microcrystalline phase. In summary, we found that for the protein sample containing ~25 mol percent of the ^{13}C,^{15}N-labeled EDTA-Cu^{2+} protein diluted in a matrix of its natural abundance diamagnetic counterpart the residual intermolecular ^{15}N-Cu^{2+} couplings contribute to a relatively small, but measurable, degree to ^{15}N PREs determined for a subset of amino acid residues; these residual intermolecular couplings were effectively quenched by further diluting the ^{13}C,^{15}N-EDTA-Cu^{2+} protein in the diamagnetic matrix, to ~10–15%. These results are expected to be quite generally applicable to structural solid-state NMR studies of other proteins modified with paramagnetic tags with ~15–20% dilution of the paramagnetic ^{13}C,^{15}N-labeled protein in the diamagnetic matrix likely providing the best compromise between the dilution factor and spectral signal-to-noise ratio, although the details of sample preparation will also depend on the size of the paramagnetic tag and the packing mode of protein molecules within microcrystals, fibers or other immobilized assemblies.

Interestingly, we have also found that regardless of the dilution factor a subset of residues distant from the EDTA-Cu^{2+} tag displayed experimentally measured longitudinal ^{15}N PREs that were systematically elevated by relatively small amounts with respect to values calculated using protein structural models. These anomalously elevated PREs are most likely caused by the availability in the protein of secondary Cu^{2+} binding sites, associated with the side-chains of aspartate and glutamate residues, combined with the small excess of Cu^{2+} ions used during the preparation of protein microcrystals in the current study. The existence of these secondary binding sites was confirmed by Cu^{2+} titration monitored by solution-state NMR, and indeed many of the amino acid residues in the vicinity of these sites were the same ones found to display the

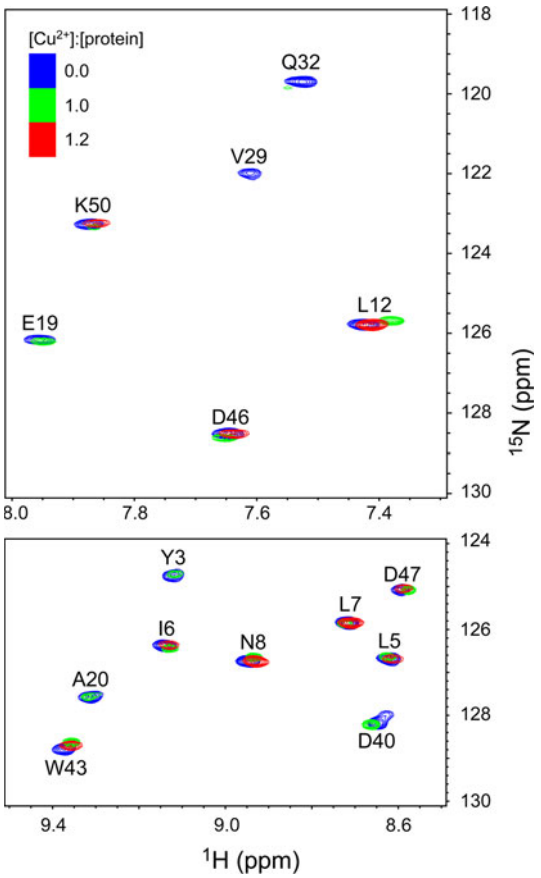

Fig. 7 Small regions of 2D ^{15}N-^{1}H HSQC solution-state NMR spectra recorded at 600 MHz ^{1}H frequency for samples containing 0.40 mM ^{15}N-K28C-EDTA GB1 and $CuCl_2$ at the concentrations of 0 mM (*blue contours*), 0.40 mM (*green contours*) and 0.48 mM (*red contours*), corresponding to Cu^{2+}:protein molar ratios of 0, 1.0 and 1.2, respectively

increased ^{15}N PREs in the solid phase. These findings suggest that the most accurate PRE measurements are likely to be obtained for protein samples prepared with stoichiometric or slightly sub-stoichiometric amounts of paramagnetic ions relative to the concentration of the high-affinity metal-binding tag.

Acknowledgments This work was supported by the National Science Foundation (CAREER Award MCB-0745754 to C.P.J) and Eli Lilly and Company (Young Investigator Award to C.P.J.). We thank Dr. Charles Schwieters for his assistance with the Xplor-NIH software.

References

Balayssac S, Bertini I, Lelli M, Luchinat C, Maletta M (2007) Paramagnetic ions provide structural restraints in solid-state NMR of proteins. J Am Chem Soc 129:2218–2219

Balayssac S, Bertini I, Bhaumik A, Lelli M, Luchinat C (2008) Paramagnetic shifts in solid-state NMR of proteins to elicit structural information. Proc Natl Acad Sci USA 105:17284–17289

Baldus M, Petkova AT, Herzfeld J, Griffin RG (1998) Cross polarization in the tilted frame: assignment and spectral simplification in heteronuclear spin systems. Mol Phys 95:1197–1207

Bertini I, Luchinat C, Parigi G (2001) Solution NMR of Paramagnetic Molecules: Applications to Metallobiomolecules and Models. Elsevier, Amsterdam

Bertini I, Luchinat C, Parigi G, Pierattelli R (2008) Perspectives in paramagnetic NMR of metalloproteins. Dalton Trans 29:3782–3790

Bertini I, Bhaumik A, De Paëpe G, Griffin RG, Lelli M, Lewandowski JR, Luchinat C (2010a) High-resolution solid-state NMR structure of a 17.6 kDa protein. J Am Chem Soc 132:1032–1040

Bertini I, Emsley L, Lelli M, Luchinat C, Mao J, Pintacuda G (2010b) Ultrafast MAS solid-state NMR permits extensive ^{13}C and ^{1}H detection in paramagnetic metalloproteins. J Am Chem Soc 132:5558–5559

Bloembergen N, Morgan LO (1961) Proton relaxation times in paramagnetic solutions. Effects of electron spin relaxation. J Chem Phys 34:842–850

Böckmann A, Meier BH (2010) Prions: En route from structural models to structures. Prion 4:72–79

Brough AR, Grey CP, Dobson CM (1993) Paramagnetic ions as structural probes in solid-state NMR: Distantce measurements in crystalline lanthanide acetates. J Am Chem Soc 115:7318–7327

Chacko VP, Ganapathy S, Bryant RG (1983) ^{13}C CP-MAS NMR spectra of paramagnetic solids. J Am Chem Soc 105:5491–5492

Clore GM, Iwahara J (2009) Theory, practice, and applications of paramagnetic relaxation enhancement for the characterization of transient low-population states of biological macromolecules and their complexes. Chem Rev 109:4108–4139

Delaglio F, Grzesiek S, Vuister GW, Zhu G, Pfeifer J, Bax A (1995) NMRPipe: a multidimensional spectral processing system based on UNIX pipes. J Biomol NMR 6:277–293

Detken A, Hardy EH, Ernst M, Meier BH (2002) Simple and efficient decoupling in magic-angle spinning solid-state NMR: the XiX scheme. Chem Phys Lett 356:298–304

Ebright YW, Chen Y, Pendergrast S, Ebright RH (1992) Incorporation of an EDTA-metal complex at a rationally selected site within a protein: application to EDTA-iron DNA affinity cleaving with catabolite gene activator protein (CAP) and Cro. Biochemistry 31:10664–10670

Ermácora MR, Delfino JM, Cuenoud B, Schepartz A, Fox RO (1992) Conformation-dependent cleavage of staphylococcal nuclease with a disulfide-linked iron chelate. Proc Natl Acad Sci USA 89:6383–6387

Goddard TD, Kneller DG (2006) SPARKY 3, University of California, San Francisco

Hediger S, Meier BH, Ernst RR (1995) Adiabatic passage Hartmann-Hahn cross polarization in NMR under magic angle sample spinning. Chem Phys Lett 240:449–456

Ishii Y, Wickramasinghe NP, Chimon S (2003) A new approach in 1D and 2D ^{13}C high-resolution solid-state NMR spectroscopy of paramagnetic organometallic complexes by very fast magic-angle spinning. J Am Chem Soc 125:3438–3439

Jahnke W (2002) Spin labels as a tool to identify and characterize protein-ligand interactions by NMR spectroscopy. Chembiochem 3:167–173

Jovanovic T, McDermott AE (2005) Observation of ligand binding to cytochrome P450-BM-3 by means of solid-state NMR spectroscopy. J Am Chem Soc 127:13816–13821

Kay LE, Keifer P, Saarinen T (1992) Pure absorption gradient enhanced heteronuclear single quantum correlation spectroscopy with improved sensitivity. J Am Chem Soc 114:10663–10665

Kosen PA (1989) Spin labeling of proteins. Meth Enzymol 177:86–121

Kupce E, Boyd J, Campbell ID (1995) Short selective pulses for biochemical applications. J Magn Reson B 106:300–303

Laage S, Lesage A, Emsley L, Bertini I, Felli IC, Pierattelli R, Pintacuda G (2009a) Transverse-dephasing optimized homonuclear J-decoupling in solid-state NMR spectroscopy of uniformly ^{13}C-labeled proteins. J Am Chem Soc 131:10816–10817

Laage S, Sachleben JR, Steuernagel S, Pierattelli R, Pintacuda G, Emsley L (2009b) Fast acquisition of multi-dimensional spectra in solid-state NMR enabled by ultra-fast MAS. J Magn Reson 196:133–141

Lee RW, Oldfield E (1982) Nuclear magnetic resonance of heme-protein crystals: structure of the heme in Physeter catodon ferrimyoglobin and an analysis of hyperfine shifts. J Biol Chem 257:5023–5029

Linser R, Fink U, Reif B (2009) Probing surface accessibility of proteins using paramagnetic relaxation in solid-state NMR spectroscopy. J Am Chem Soc 131:13703–13708

Liu K, Ryan D, Nakanishi K, McDermott AE (1995) Solid-state NMR studies of paramagnetic coordination complexes: a comparison of protons and deuterons in detection and decoupling. J Am Chem Soc 117:6897–6906

Liu K, Williams J, Lee H, Fitzgerald MM, Jensen GM, Goodin DB, McDermott AE (1998) Solid-state deuterium NMR of imidazole ligands in cytochrome c peroxidase. J Am Chem Soc 120:10199–10202

McDermott A (2009) Structure and dynamics of membrane proteins by magic angle spinning solid-state NMR. Annu Rev Biophys 38:385–403

Nadaud PS, Helmus JJ, Hofer N, Jaroniec CP (2007) Long-range structural restraints in spin-labeled proteins probed by solid-state nuclear magnetic resonance spectroscopy. J Am Chem Soc 129:7502–7503

Nadaud PS, Helmus JJ, Kall SL, Jaroniec CP (2009) Paramagnetic ions enable tuning of nuclear relaxation rates and provide long-range structural restraints in solid-state NMR of proteins. J Am Chem Soc 131:8108–8120

Nadaud PS, Helmus JJ, Sengupta I, Jaroniec CP (2010) Rapid acquisition of multidimensional solid-state NMR spectra of proteins facilitated by covalently bound paramagnetic tags. J Am Chem Soc 132:9561–9563

Nayeem A, Yesinowski JP (1988) Calculation of magic-angle spinning nuclear magnetic resonance spectra of paramagnetic solids. J Chem Phys 89:4600–4608

Otting G (2010) Protein NMR using paramagnetic ions. Annu Rev Biophys 39:387–405

Pines A, Gibby MG, Waugh JS (1973) Proton-enhanced NMR of dilute spins in solids. J Chem Phys 59:569–590

Pintacuda G, Giraud N, Pierattelli R, Bockmann A, Bertini I, Emsley L (2007) Solid-state NMR spectroscopy of a paramagnetic protein: assignment and study of human dimeric oxidized Cu^{II}-Zn^{II} superoxide dismutase (SOD). Angew Chem Int Ed 46:1079–1082

Renault M, Cukkemane A, Baldus M (2010) Solid-state NMR spectroscopy on complex biomolecules. Angew Chem Int Ed 49:8346–8357

Schwieters CD, Kuszewski JJ, Tjandra N, Clore GM (2003) The Xplor-NIH NMR molecular structure determination package. J Magn Reson 160:65–73

Shaka AJ, Keeler J, Freeman R (1983) Evaluation of a new broadband decoupling sequence: WALTZ-16. J Mag Reson 53:313–340

Solomon I (1955) Relaxation processes in a system of two spins. Phys Rev 99:559–565

Spooner PJR, Veenhoff LM, Watts A, Poolman B (1999) Structural information on a membrane transport protein from nuclear magnetic resonance spectroscopy using sequence-selective nitroxide labeling. Biochemistry 38:9634–9639

States DJ, Haberkorn RA, Ruben DJ (1982) A two-dimensional nuclear Overhauser experiment with pure absorption phase in four quadrants. J Magn Reson 48:286–292

Su Y, Mani R, Hong M (2008) Asymmetric insertion of membrane proteins in lipid bilayers by solid-state NMR paramagnetic relaxation enhancement: a cell-penetrating peptide example. J Am Chem Soc 130:8856–8864

Tycko R (2011) Solid-state NMR studies of amyloid fibril structure. Annu Rev Phys Chem 62:279–299

Ubbink M, Worrall JAR, Canters GW, Groenen EJJ, Huber M (2002) Paramagnetic resonance of biological metal centers. Annu Rev Biophys Biomol Struct 31:393–422

Walter TH, Oldfield E (1987) Magic-angle sample-spinning NMR spectroscopy of an antiferromagnetically coupled copper formate dimer. J Chem Soc Chem Commun 646–647

Wickramasinghe NP, Kotecha M, Samoson A, Past J, Ishii Y (2007) Sensitivity enhancement in ^{13}C solid-state NMR of protein microcrystals by use of paramagnetic metal ions for optimizing ^{1}H T_1 relaxation. J Magn Reson 184:350–356

Wickramasinghe NP, Parthasarathy S, Jones CR, Bhardwaj C, Long F, Kotecha M, Mehboob S, Fung LWM, Past J, Samoson A, Ishii Y (2009) Nanomole-scale protein solid-state NMR by breaking intrinsic ^{1}H T_1 boundaries. Nat Methods 6:215–218

Zhang Y, Sun HH, Oldfield E (2005) Solid-state NMR Fermi contact and dipolar shifts in organometallic complexes and metalloporphyrins. J Am Chem Soc 127:3652–3653